

# RGB cameras failures and their effects in autonomous driving applications

Andrea Ceccarelli, Francesco Secci

**Abstract**— RGB cameras are one of the most relevant sensors for autonomous driving applications. It is undeniable that failures of vehicle cameras may compromise the autonomous driving task, possibly leading to unsafe behaviors when images that are subsequently processed by the driving system are altered. To support the definition of safe and robust vehicle architectures and intelligent systems, in this paper we define the failure modes of a vehicle camera, together with an analysis of effects and known mitigations. Further, we build a software library for the generation of the corresponding failed images and we feed them to six object detectors for mono and stereo cameras and to the self-driving agent of an autonomous driving simulator. The resulting misbehaviors with respect to operating with clean images allow a better understanding of failures effects and the related safety risks in image-based applications.

**Index Terms**— autonomous driving; RGB camera; failures; obstacles detection; driving simulation; image-based applications

## 1 INTRODUCTION

Autonomous driving is attracting growing attention in recent years, with ever-increasing demand and investments from the industry [17]. The objective of an autonomous driving system is to drive by itself without requiring help from a human: the vehicle detects the environment, locates its position, and operates to get to the specified destination safely.

Sensor technology, data-fusion and inference algorithms as Artificial Intelligence and Machine Learning (AI/ML) applications are the enabling technologies that play a cornerstone role in autonomous driving systems. These are involved in the majority of the essential tasks for safe driving such as sensor-fusion, environment representation, scene understanding, semantic segmentation, tracking, object detection and recognition [15].

Amongst sensors, the RGB (red, green and blue) camera is acknowledged as the most commonly used and an irreplaceable one [15]. In fact, despite cameras have the known disadvantages of strong sensitivity to external illumination and limited field of view, visual recognition systems are amongst the most solid applications of autonomous driving [33]. Vehicle cameras are already exploited in many applications such as traffic sign recognition, lane detection, obstacle detection, etc. [15], [16], [17]. Additional prospective applications are being researched; for example, at intersections, knowing the location of pedestrians and bicyclists can allow the car to make sophisticated precedence decisions [16]. Also, cameras are amongst the cheapest solutions to build autonomous driving systems that are capable of sensing the surroundings [17].

When the images provided by the camera are degraded, fatal accidents may occur. The trained agents of the AI/ML applications responsible for the elaboration of inputs may

rely on biased data and consequently lead to wrong (unsafe) decisions.

A considerable number of works explore how to make the trained agents robust to artificially crafted or accidentally manipulated input images [35], [36], [37], and how to secure a camera from direct attacks that may disrupt the proper behavior of the camera itself [18], [19]. In fact, even slight alterations of the images may alter the output of the trained agent [39]. However, few or no works focused on the attentive identification of a realistic and complete set of accidental modifications of images from a failed RGB camera. To the best of our knowledge, existing works consider a credible set of image alterations but without a systematic analysis of what are the possible malfunctions of a camera and consequently without a shared failures model and software libraries for its reproduction.

We observe that cameras failures and their effects on the overall system should be systematically studied to fully understand the resulting safety threats at system-level, and possible mitigations should be identified carefully. Such study would benefit system and software engineers, both for architecting of system and for robustness assessment of image-based AI/ML applications.

To walk towards this goal, the contributions of this paper is organized in four parts. *First*, we identify failure modes for vehicle cameras in the domain of autonomous driving, by analyzing the different failures, their causes and their potential effects on the system. We achieve this goal applying an FMEA (Failure Modes and Effects Analysis, [14]) on the components of an RGB camera, assuming the camera is located on a vehicle. *Second*, we review existing mitigations; this review shows that while mitigations exist for essentially any individual failure, an orchestrated approach to the whole failure set is still missing. *Third*, we exercise trained agents for object detection on failed images, to measure the performance drop due to failures manifestation. For this scope, we alter images from the KITTI Vision Benchmark Suite for autonomous driving [75], [76]

- Andrea Ceccarelli is with the Department of Mathematics and Informatics, University of Florence, Viale Morgagni 65, 50134, Florence, Italy. E-mail: andrea.ceccarelli@unifi.it.
- Francesco Secci is with the Department of Mathematics and Informatics, University of Florence, Viale Morgagni 65, 50134, Florence, Italy.

according to our failure modes, using a python library that we developed and that is publicly available at [9]. At this point, we execute six object detector on the modified images, measuring the resulting detection capability in terms of Average Precision [77]. Further, we confirm the failures effects and discuss the associated safety risks using a self-guiding agent for autonomous driving. In this case, we inject failures in the frontal camera of a vehicle simulated in the Carla autonomous driving simulator [1], where the trained agent from [3] is running. This allows discussing the misbehavior of the trained agent mainly in terms of number of collisions.

This work is an extended version of the paper in [78]. The most noticeable additional contributions are i) the analysis of failures effects on the six object detectors operating on an image dataset for autonomous driving; ii) the revision of the python library with the introduction of the flare failure and the revision of several others, and ii) the inclusion of additional configurations for the injection of failures, from the 31 in [78] to a total of 130 in this paper.

The rest of the paper is organized as follows. In Section 2 we present the fundamentals that are at the basis of our work. In Section 3 we detail the identified failures of camera components, their effects on the output image, and possible mitigations. In Section 4 and Section 5 respectively we execute object detectors on altered images from the KITTI dataset, and we inject the failures in the frontal camera of a simulated vehicle that is driving autonomously, and we discuss the impact of failures. Finally, in Section 6 we review related works and in Section 7 we define conclusions.

## 2 BACKGROUND NOTIONS

We present background notions that are at the basis of our work. In Section 2.1 we define the architectural structure of an RGB camera (simply called camera, from now on) that we use as reference in our work, and in Section 2.2 we describe the FMEA methodology that we apply to identify camera failures.

### 2.1 Architecture of a Camera

We consider a camera structured in five components (Fig. 1): lens, camera body, Bayer filter, image sensor and ISP (Image Signal Processor) [27]. These five components contribute to the creation of the output image.

**Lens.** Photographic lenses are devices capable of collecting and reproducing an image [7]. The lens is the component that has the greatest impact on the quality of the images. The photographic lens can be composed of one or more lenses and/or reflectors as for example systems of concave



Fig. 1. A camera and its components: Lens, and the Camera Body composed of Bayer Filter, Image Sensor, Image Signal Processor.

and convex mirrors, often also combined with diopters. The fundamental factor that distinguishes one lens from another is primarily the focal length, which allows dividing them into macro categories. A second factor that characterizes the lens is brightness. A third distinguishing factor are macros: a macro lens has the ability to focus from infinity to 1:1 magnification that is, the size of the image in real life is the same size as it is reproduced on the sensor. Another relevant factor is the focus: this can be manual or automatic. The lens also contains a minimum of electronics, necessary for the focus motor (when automatic) and for zooming [20], and also they may or may not be stabilized.

**Camera Body.** The camera body is the container of all the electronics of the camera. The Bayer filter, the image filter and the ISP are here contained. Typically, the functions of the camera body are securing the device and protecting inner components from exposure and contact with the outside. For example, the case protects the sensor from light and other possible sources of damage.

**Bayer Filter.** The Bayer filter (or Bayer pattern) is used for the acquisition of digital images [71]. The photodiodes in an image sensor are color-blind by nature: they can only register shades of gray. To obtain the color in the image, they are covered with different color filters: red, green and blue (RGB) according to the model designated by the Bayer filter. This filter groups the sensors for the three fundamental colors RGB in cells of 2x2 photosites: each cell contains two green elements, one red element and one blue element (Fig. 2). Each pixel is filtered to register only one of the three colors: to obtain a color image, various demosaicing algorithms can be used that interpolate a set of complete red, green and blue values for each pixel. These algorithms use the surrounding pixels to estimate the value for a particular pixel [70].

**Image Sensor.** The image sensor is the transducer that converts the image into its representation or electrical coding. Essentially, it is a silicon chip capable of capturing and measuring light i.e., the quantity of photons which reach the chip. The sensor surface is made up of millions of tiny receivers arranged in a regular grid; these receivers, also called photosites, are the microsensors that carry out the

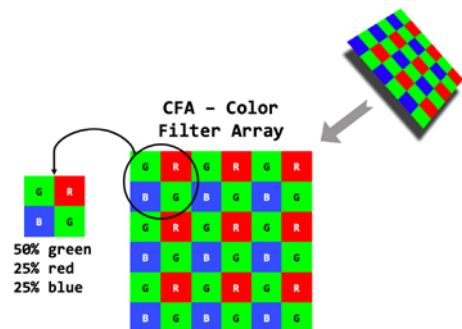


Fig. 2. Scheme of a Bayer filter. On the left, a sample cell of 2x2 photosites (BGGR pattern). In digital imaging, a color filter array (CFA), or color filter mosaic (CFM), is a mosaic of tiny color filters placed over the pixel sensors of an image sensor to capture color information [41].

conversion from photons to electrons. Each individual receiver is able to supply an electrical charge proportional to the number of photons that hit it. The detected charge is then converted by a special analog-digital conversion circuit into a numerical value. Each of the values obtained from the photosites will constitute a pixel of the obtained image.

There are currently two types of image sensors on the market: CCD (Charge Coupled Device) and CMOS (Complementary Metal Oxide Semi-conductor). Both are based on the concept of converting the charge of each photosites into a digital format using an ADC (Analog to Digital Converter), but they differ in how the information is processed. In fact, for CCD sensors, the information on the charge is taken from the photosites row by row and stored in a register whose content is passed to an amplifier and subsequently to the ADC. After the row has been fully processed, it is eliminated from the exit register and the next row that undergoes the same treatment is loaded. Instead in CMOS sensors, together with photosites a series of transistors have also been integrated which perform an amplification and conversion of the charge into voltage. Using a matrix structure, it is possible to individually select each photosites through its  $[row, column]$  coordinates, and then send the voltage to an ADC that performs the conclusive digital conversion [6], [42].

**ISP.** The Image Signal Processor is a type of specialized media processor or Digital Signal Processor (DSP), used for image processing in digital cameras as well as other devices [42]. Its functions are multiple and fundamental for the final result after a first acquisition of the image, such as: demosaicing, correction of the image sensor, noise reduction, image sharpness correction, resizing the image, lens distortion correction, chromatic aberration correction, image compression and JPEG encoding, video compression, audio processing / compression / encoding and more [42].

## 2.2 Principles of FMEA

The Failure Mode and Effects Analysis (FMEA, [14]) is a widely-used reliability management technique designed to identify potential failures of a component or a process, understand the effects of these failures, assess the risk associated with these failure modes and ultimately classify problems in terms of importance [4]. This failure identification allows choosing and implementing corrective actions to address the most serious potential failures. Usually performed analytically, an FMEA is composed of four stages [4], [5]: i) identify all known or potential failure modes of a system; ii) confirm the *causes* and *effects* of each failure; iii) rank the recognized failures by their *risk*, defined as a combination between the probability of occurrence of a failure and the severity of the latter; iv) take remedial actions for the highest risky failures.

The assumption underlying the application of the FMEA is the principle according to which the risk is related not only to the probability that a failure occurs, but also the seriousness of its consequences and ability to avoid or mitigate it. Ultimately, FMEA provides a knowledge base of

the failure modes and information on their effects that can be used as a resource for future troubleshooting activities [4], [5], [14], which matches the objectives of our work and it is the reason why this technique was selected.

## 3 ANALYSIS OF CAMERA FAILURES

We consider a frontal camera of a vehicle organized in the five components discussed in Section 2.1, and we assume that output images are then processed by image-based AI/ML applications. We exercise the FMEA on the components of the camera. The application of the FMEA identifies the failure modes of the camera components, the cause of such failures, and their resulting effect at camera-level i.e., on the output image. Further, we complement this list with a literature review on camera failures, to assure that no relevant failure modes are left out. With respect to the usual analytical application of FMEA, due to the absence of reference data, we could not associate credible ratings on the risk matched to the individual failures (this is in-line with acknowledged limitations of risk ratings in FMEA [4]). However, we mitigate this gap through Section 4 and Section 5, via the execution of image-based applications for autonomous driving.

In Section 3.1 we list the failures in alphabetic order; we assign an evocative name to each failure, that we will use in the rest of the paper. In Section 3.2 we summarize the failures, and we report state-of-the-art mitigations.

### 3.1 List of identified failures

**Banding.** In this failure, many parallel horizontal and/or vertical lines becomes visible in the produced image. The lines are more visible when looking at the darker colors, although they can be also perceived on lighter ones. Another type of banding can be seen on images where the plain background color degrades, from the point of view of tones, in lighter colors: this is typically called dithering [59]. Figure 3 shows the Banding failure injected into Fig. 4a. Only a portion of the banded image is shown, to make the banding effects clearly visible to the naked eye. Banding failures manifest in the image sensor.

**Brightness.** These failures represent the brightness alteration, from its minimum (black image) to its maximum (white image) limits, that can happen with the breakdown of fundamental components of the lens such as the shutter, the diaphragm or the iris (Fig. 4b). For example, if the shutter has a malfunction that does not allow the entrance of the correct amount of light through the lens, brightness could be altered, from entirely black to entirely white.



Fig. 3. Banding applied to Fig. 4a: dark lines become visible.

These brightness failures manifest in the lens component.

**Blurred.** Blur may occur if the image captured by the device is not in focus (Fig. 4c) [69]. Especially in autonomous driving, it is of fundamental importance that the captured images are of good quality and therefore in focus. This is clear if we think that the image-based AI/ML applications make decisions regarding the vehicle's movement, based on the information content of the camera images. Blurred failures manifest in the lens component.

**Brackish/Salt-Water.** The brackish phenomenon is common in coastal areas and puts a strain on the durability of the materials if not treated with suitable products and/or not maintained over time [6]. The corrosive power of water and air given by the substantial percentage of salt may damage the lens and also the camera body itself, to the extent that external agents may enter the circuits [43]. In the worst scenario, this can affect image acquisition. The image may be altered in various ways; we refer to the description of all the other failures effects for a complete characterization of Brackish/Salt-Water effect. This failure manifests in the lens and camera body.

**Bright Lines.** This failure is rather rare with the current knowledge and technology. The produced images could show bright vertical and/or horizontal lines, also clearly distinguishable with the naked eye. The cause of these lines is due to the use of LIDARs: this laser technology emits a light intensity (not visible to the human eye) that can seriously damage the camera's image sensor. This failure may manifest in the image sensor.

**Broken Lens.** One or more internal or external lenses may break, for example because of mechanical stresses due to vehicle jolts or the impact with gravel throw-up by the tires of nearby vehicles. The camera regularly outputs the image, but it will include an additional line (in case of a scratch) or more complicated patterns (Fig. 4d). This failure manifests in the lens component.

**Broken VR.** In this case, the malfunction of the component that deals with the reduction of vibrations (VR) is considered. This is located in the lens and it is common on many camera models. Its malfunction causes out of focus images: for this reason, the effects of this failure are similar to the Blurred ones. Broken VR manifests in the lens component.

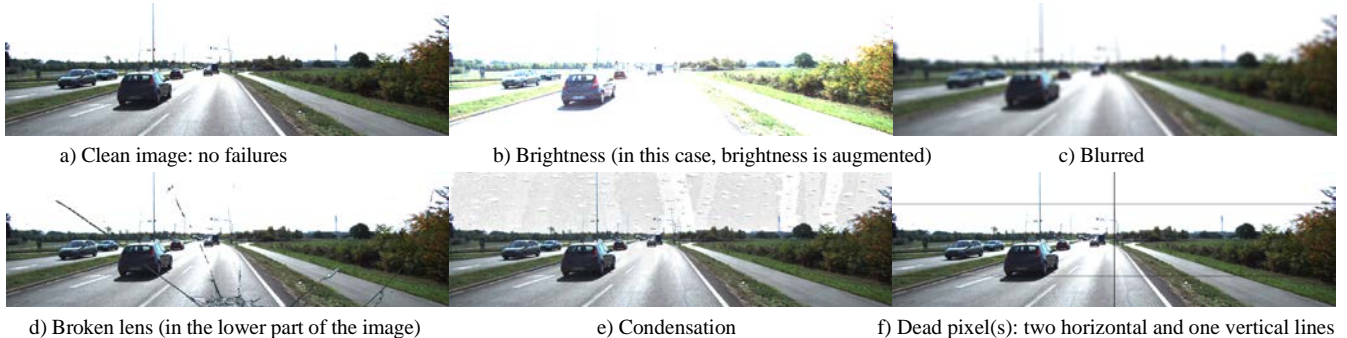


Fig. 4. Visual effect of five different failures on the output image of a frontal camera. Failures are applied to the image in 4a, that is from the KITTI Vision Benchmark [75], [76] suite.

**Condensation.** When the outside air temperature drops sharply, condensation may appear on the lenses. Condensation, or humidity, degrades the images (Fig. 4e). The image is acquired in the correct way, but each image may have heavy changes due to halos on the lenses [72]. If humidity penetrates inside the camera body, it may cause malfunctions and it may also preclude the entire operability of the device. Condensation failure manifests in the lens and camera body.

**Dead Pixel.** In this failure, the output images have one or more defects of a pixel size. While this failure manifest in the image sensor, we call it dead pixel, because it has the same visual effect of the common failure that can be noticed on LCD displays, when a pixel stops working properly and it appears as a black spot on the screen. A single dead pixel may not preclude the good interpretation of the captured images by the AI/ML applications, despite a deliberately modified pixel may actually do so [39]. Obviously, several dead pixels (e.g., an extreme case is in Fig. 4f) have higher chances to drop the accuracy of the AI/ML application that uses the image.

**Dirty (Internal – External).** This failure (Fig. 5a) concern debris of various kinds and sizes (most typically, dust and dirt) which deposits on the internal or external lenses [72]. The most significant difference is that the external dirt can be removed, usually by cleaning the first lens of the objective (i.e., the most external lens). Instead, removing the internal dirt requires more time and, sometimes, specialized personnel [44]. Dirty-related failures manifest in the lens component.

**Electrical Overload.** The excessive and dangerous temperature increase of the conductors due to an electrical overload could damage, and most likely break, the electrical parts in the camera body. A device with this generic electrical problem may stop working or find itself in a state where images cannot be processed [44]. The resulting effect is that the images are produced incorrectly or, most likely, not produced at all. Electrical overload may manifest in the camera body.

**Flare.** The structure itself of the lenses group creates flare (Fig. 5b). Flare is due to the reflection of the sun or other light sources on the lenses. The resulting image shows one or more spots of various colors, placed on an imaginary

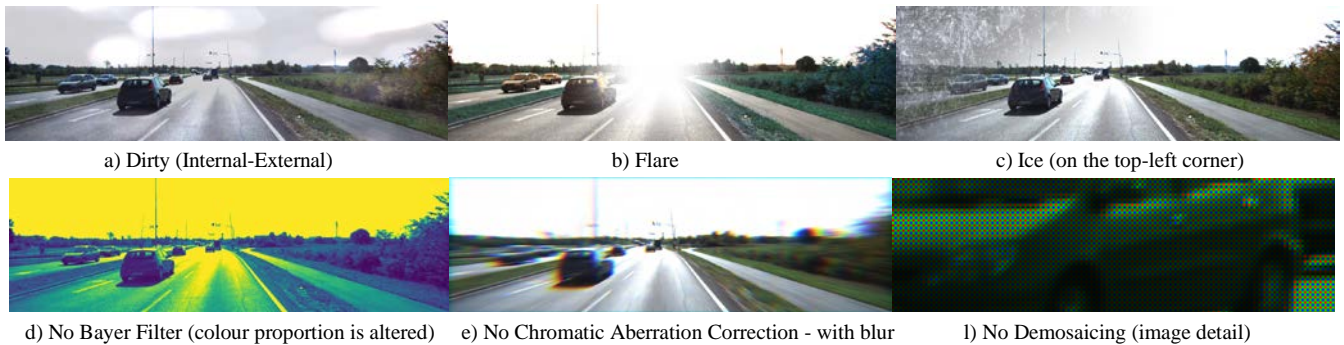


Fig. 5. Visual effect of six different failures applied to Fig. 4a.

line. Obviously, these spots can cover details in the images: the subsequent processing steps, even if the image is captured correctly, will be influenced by the presence of these spots. Flare is difficult to eliminate completely also with the modern technology, that sets a series of lenses slightly spaced one from each other, and each with a specific task. Flare failure manifests in the lens component.

**Heat.** This type of failure relates to the heat that the lens or camera body can suffer in their operational life. In extreme cases, excessive heat could lead to the evaporation of the lubricating liquids of the moving parts (e.g., zoom). As a result, the use of the zoom (if present) and of other sub-components that are intended to make the image as clear as possible (e.g., the focus tools) may be precluded. As for Brackish/Salt-Water, the image may be altered in various ways and we refer to the description of all the other failures effects for a complete characterization of heat effects. The heat failure manifests in the lens and camera body.

**Ice.** Ice can be the cause of several camera malfunctions. In fact, this can break the external materials of camera lens and camera body. Furthermore, the external lens can be covered with a blanket of ice that prevents the acquisition of images (Fig. 5c). The Ice failure manifests in the lens and the camera body.

**No Action.** A failed ISP does not respond and therefore the processing of the acquired image does not take place: the image remains in raw format, without any type of processing. As effect, the camera does not transmit anything to the other processing components of the vehicle. This failure manifests in the ISP.

**No Bayer Filter.** Without a Bayer Filter properly functioning, the produced image would result in wrong colors (for example, in Fig. 5d, colors are altered using the RGB coefficients from ITU-R BT.601 [79] to generate achromatic images). The following phases would unavoidably process chromatically wrong images. This failure manifests in the Bayer filter.

**No Chromatic Aberration Correction - Incomplete Chromatic Aberration Correction.** It refers to the case that the ISP fails to (fully or partially) apply the removal of chromatic aberration on the acquired image. In optics, axial chromatic aberration is a defect in the formation of the

image, due to the different refractive values of the light wavelengths that passes through the optical instrument [67]. It is a defect which may affect all optical lens systems, to varying degrees. This failure leads to images with colored halos on the edges of the subjects: the images show "fringes" of various colors (mostly purple) and a sort of blur (Fig. 5e). This failure manifests in the ISP.

**No Demosaicing - Incomplete Demosaicing.** In No Demosaicing, we consider the case in which the image is acquired in RAW format (Fig. 5f). This means that the demosaicing process has not been carried out and therefore the image is presented with each pixel containing a red, green or blue value. In this case the Bayer array has not yet been interpreted and the image is more pixelated than normal. The prevalence of the greenish hue, also visible in Fig. 5f, is due to the high percentage of green parts, that is double the percentage of the red and blue parts, following the BGR pattern in the Bayer filter as previously shown in Fig. 2. This failure manifests in the ISP.

**No Lens Distortion Correction - Incomplete Lens Distortion Correction.** This failure may affect only vehicles which mount cameras with wide-angle lens [21], [73], which tend to deform the image. In this case, the captured image appears as mapped around a sphere that is more protruding towards the observer, in the center of the image. If the conversion to normal proportions (natural symmetric) is not successful, the image may freeze in this processing phase and the system may be in a stalled state. Alternatively, if the output image is incorrectly processed, the AI/ML applications may use images with surrounding objects of distorted proportions and shapes. This failure manifests in the ISP.

**No Noise Reduction - Incomplete Noise Reduction.** The device captures the image, but during the processing phases (noise reduction) there is an error that prevents the correct removal of the noise e.g., Fig. 6a. This failure manifests in the ISP.

**No Sharpness - Incomplete Sharpness.** In this case, the processing of the captured images fails during the sharpness correction phase. This affects the ability of a camera to identify and define the separation limit between two contiguous areas that have different brightness and/or color (Fig. 6b). This failure manifests in the ISP.



Fig. 6. Visual effect of three different failures applied to Fig. 4a.

**Rain.** It refers to the case in which there are small spots on the images due to the deposit of water drops on the external lens [72] (Fig. 6c). The elimination of these stains can be considered trivial when the vehicle is parked and without rainfall. However, given the weather variability that a vehicle can encounter, we cannot only consider such simple case. This failure manifests in the lens.

**Sand.** Because of sand, there may be a possible corrosion of the external sub-components of the lens (percentage of salt in the sand), with the consequent introduction of external agents inside the device, and to the extent that the camera may not capture exact images. In fact, sand could block sub-components which have the purpose of making the image as clear as possible (tools for focusing, zooming, etc.). The effect on the output image (when sand is on the lens) is similar to Dirty Internal-Dirty External. This failure manifests in the lens and camera body.

**Spots.** This failure occurs when small particles of dust (or other type of material) settle on the Image Sensor. This deposit means that small spots, or shadows, are visible above the light colors on the output image. Such shadows are mostly circular in shape and are very common for amateur photography, particularly when using multiple lenses. In fact, while operating on the camera for maintenance, external agents of imperceptible size may enter and settle on the exposed Image Sensor [74]. The failure effect is similar to the Dirty Internal-Dirty External. This failure manifests in the image sensor.

**Water.** If water enters the lens or the camera body, the electrical components can fail and most likely no longer acquire images, or acquire them without any content [72]. This failure manifests in the lens and camera body.

**Wind.** We consider those parts of the component with cavities that, due to the force of the wind (while the vehicle is in motion or parked), could lead to minimal external damage and the subsequent infiltration of various agents inside the camera. The acquisition of images could therefore be incorrect: lens may move and images may be shifted or cut, etc. This can be considered very rare for a vehicle camera. This failure manifests in the lens and camera body.

### 3.2 Summary of the Analysis

Table I recaps the failure modes and the involved camera components. Further, we add a discussion on possible mitigations that can be implemented in the camera for each individual failure.

## 4 EFFECTS ON DETECTION APPLICATIONS

We study the effects of failures by exercising six object detectors on images captured by an RGB vehicle camera. The images are from the KITTI Vision Benchmark Suite [75], [76] for autonomous driving, and the object detectors are amongst the ranked solution on such suite for mono and stereo cameras. To perform the injections, we developed a Python library available at [9]. All the failed images and the detection results are available at [10].

### 4.1 KITTI image dataset and target metrics

The KITTI Vision Benchmark Suite (hereafter, just KITTI) includes images showing a variety of street situations captured from a moving platform driving around the city of Karlsruhe. A set of 7481 images is provided with the ground truth, defined through labels that contain the bounding boxes of objects as cars, pedestrian, cyclists amongst others. As all images are captured by a stereo camera (i.e., two parallel sets of images are provided), they can be used for both 2D and 3D object detection. A similar set of images is intended for fair testing and comparison of object detectors, and ground-truth labels are not released.

KITTI includes a benchmark to measure object detection performance based on the average precision AP [77]. AP summarizes the shape of the precision/recall curve, and it is defined as the mean precision at a set of  $n$  equally spaced recall levels. Value  $n$  is set to 11 in [77], while it is set to  $n=40$  in KITTI. In other words, we have that:

$$AP = \frac{1}{40} \sum_{r \in \{0, \frac{1}{40}, \frac{2}{40}, \dots, 1\}} p_{interp}(r)$$

where the precision  $p$  at each recall level  $r$  is interpolated by taking the maximum precision measured for which the corresponding recall exceeds  $r$  [77].

We compute AP using the standard KITTI configuration for cars detection, which confirms detection if there is at least an overlap of 70% between the ground-truth bounding boxes and the generated bounding boxes. We retrieve the AP values from the output of the object detector if available, or by processing the produced bounding boxes using the tool at [80].

### 4.2 The selected object detectors

We selected six object detectors by exploring the ranking for 2D and 3D object detection available on the KITTI website. The mandatory criteria for the selection are: i) source code or trained model publicly released; ii) usage of RGB cameras only (no point clouds); iii) not older than five

TABLE I  
FAILURE MODES, FAILURES APPORTIONMENT TO THE CAMERA COMPONENTS, AND DISCUSSION ON MITIGATIONS.

Failure name	Comp.	Identified mitigations and practises
Brightness (and black, white)	LENS	Brightness, if detected, can be corrected to a certain extent at post-processing. Entirely black or entirely white images can be detected easily, but it is obviously difficult to recover the original image.
Blurred		Various methods of removing or correcting image blurring exist [45], [46]. For example, Cai et al. [45] formulates the blind blurring as a new joint optimization problem, which simultaneously maximizes the sparsity of the blur kernel and the sparsity of the clear image.
Broken lens		A broken lens may be detected through image processing, but it may be difficult to re-create a clean image.
Broken VR		Methods similar to blur removal [45], [46] are applicable for this failure.
Dirty (internal-external)		Image processing solutions can remove localized rain and dirt effects from a single image [48]. For example, physics-based methods [47] can remove dust and dirt effects from digital photographs and videos.
Flare		Lens artifacts like lens flare and ghosting can be reduced or removed at post-processing [49] from a single input image to restore the correct image.
Rain		For the mitigation of this failure, we refer to the same observations of Dirty and to [48].
Condensation	LENS-CAMERA BODY	Various works e.g., [50], [51], [52], address the problem of avoiding or removing condensation inside cameras.
Heat		Against desert and very cold temperatures, there are commercial solutions such as the video surveillance camera AXIS Q60-C PTZ [28] that meets the military standard MIL-STD-810G [60].
Sand		This failure needs to be prevented with proper casing of the camera.
Ice		Camera devices to heat lenses [53] prevent or at least reduce condensation of moisture.
Water		This failure needs to be prevented with proper casing of the camera.
Brackish/Salt-water		Approaches exist specifically to prevent corrosion of the surfaces in contact with seawater, brackish water, or fresh water [54].
Wind		
Electrical overload		These failures need to be prevented e.g., with proper casing of the camera, reliable control circuits and reliable sensors.
No Bayer filter	BAYER FILTER	
Banding	IMAGE SENSOR	There are various ways to reduce visual effects of banding e.g., by applying dithering patterns [59].
Bright lines		This failure is generally mitigated by the current knowledge and technology, and it is now rare.
Dead pixel		It is possible to detect dead pixels with solutions implementable directly in the embedded device [57]; circuits to correct dead pixels can be fabricated on a single integrated chip [58].
Spots		Many image processing methods remove blemishes e.g., Zamfir et al. [55] detect blemishes and compute their physical appearance (size, shape, position and transparency) in an image as a function of camera settings, while Steinberg et al. [56] process images to automatically correct dust.
No action	ISP	It may be easy to detect this failure at system level, but it is not possible to recover the image.
No chrom. aberration correction		Chromatic aberration effects can be reduced e.g., with image processing [22], [67].
No demosaicing		Several efficient ways for demosaicing exist as [61], [62]; however it is difficult to recover the image in case of demosaicing failure.
No lens distortion correction		Lens distortion can be measured and detected [65], and it can be corrected with image processing [64], [66].
No noise reduction		
No sharpness correction		Several solutions to reduce or remove noise and sharpness are available, also in commercial tools. Solutions that operate at sensor-level also exist e.g., [63], [29].

years i.e., 2016; iv) output must include bounding boxes in the KITTI format. With this last criterion, we can sample the individual image outputs to verify that low APs are caused by wrong detections and not because of processing issues.

We select four object detectors for mono cameras (FastBox, SqueezeDet, SqueezeDet+, ResNet50), and two for stereo cameras (DSGN, Disp R-CNN). In the following description of the object detectors, we focus on image data augmentation used during training. In fact, some augmentation techniques enlarge the training set by adding effects analogous to some of the failures we reported, and they may increase robustness against specific camera failures.

FastBox [81] is designed to achieve a high detection

performance at a very fast inference speed, and it is able to jointly perform road segmentation, car detection and street classification. We apply the KittiBox scripts at [82] to train and execute FastBox. Regarding image data augmentation, color features are augmented by applying random brightness and random contrast to the images, while spatial features are distorted by applying random flip, random resize and random crop.

SqueezeDet and SqueezeDet+ [83] are designed to be small and fast, with also a focus on energy efficient. They are both convolutional neural networks based on SqueezeNet [84]; SqueezeDet+ is a variation of SqueezeDet, where a more powerful SqueezeNet is adopted.

ResNet50 is a variant of the above, where the

convolutional layers of the ResNet50 [85] network are used. Image data augmentation techniques used on SqueezeDet, SqueezeDet+ and ReNet50 are only random cropping and flipping.

DSGN [87] is an end-to-end stereo-based 3D object detection pipeline, which relies on space transformation from 2D features to achieve a 3D structure. The image data augmentation used is horizontal flipping only.

Disp R-CNN [88], which also operates on stereo cameras, considers 3D object localization as a learning-aided geometry problem rather than an end-to-end regression problem. It extends stereo-mask R-CNN [90], and its main characteristics is that it treats the object Region of Interest [89] as an entirety rather than independent pixels. The only reported image data augmentation is the image flip of stereo-mask R-CNN.

### 4.3 Failures simulation and configuration

From the failure modes in Sect. 3, we define 130 failures configurations, reported in Table II. It should be noted that some failures alter the image in a similar way, and

consequently we group failures that have similar effects on the output image. This applies to the Blurred and the Broken VR failures (we will consider only the first one, from now on), and to the Dirty and Spots failures (again, we will consider only the first one). Further, we ignore failures whose effect is either i) not providing an output image (Electrical Overload, No Action, Water), or ii) not univocally determined (Brackish/Salt-Water, Heat, Sand). We exclude Bright Lines and Wind as we believe they are very rare for vehicles cameras. We exclude No Lens Distortion correction as the images are not collected with wide-angle lenses.

### 4.4 Experiments and results

We split the 7481 labelled KITTI images in 6891 images for training and 500 images for validation. The test set is not defined, because a separate test set is available for KITTI, whose labels are not disclosed: this is the same approach adopted in the papers describing the object detectors e.g., [81], [83].

TABLE II – FAILURES IMPLEMENTED, IMPLEMENTATION DETAILS, AND SELECTED CONFIGURATIONS.

Failures	Implementation details	Configurations (with acronyms)
Banding	We use the PIL Image Module [12] <code>resize()</code> and <code>blend()</code> methods to superimpose images with dark stripes in [9]	BAND1, BAND2: two different banding effects are applied, by superimposing two different images with dark stripes
Blurred (and Broken VR)	Blur is added using <code>cv2</code> [11] method <code>cv2.blur(img,(i,i))</code> , where $i$ is the blur level	BLUR: we introduce 25 different levels of blur, with $(i, i)$ ranging from (1,1) i.e., very light blur, to (25,25) that is a very strong blur
Brightness	Brightness is modified using PIL <code>ImageEnhance</code> module ( <code>ImageEnhance.Brightness</code> ) [12]	BRIGHT: we experiment with 10 different levels of brightness ranging from 0 (black image) to 15 (almost white)
Broken Lens	Failures are simulated using the PIL Image Module [12] and images of broken lens, dirt, rain drops, condensation, ice on lens that are superimposed to the original image. This is done either using PIL <code>paste</code> or <code>blend</code> methods, respectively if the image to be superimposed is transparent or not. PIL <code>resize</code> and brightness adjustments are used as needed, to achieve the required effect	BRLE: we try 16 configurations, by superimposing 16 different images of scratched lens from [91]
Condensation		COND: we try 3 configurations, by superimposing 3 transparent images representing condensation on lens available at [9]
Dirty (and Spots)		DIRTY: we try 36 configurations, by superimposing 36 different images representing dirt on lens from [91]
Ice		ICE: we try 4 configurations, by superimposing 4 different transparent images representing ice on lens available at [9]
Rain		RAIN: we try 5 configurations, by superimposing 5 different transparent images representing rain on lens available at [9]
Dead pixel	We change the color channel with <code>cv2</code> [11]. It is sufficient to set to (0,0,0) the image pixels that should appear black	DEAPIX1, DEAPIX50, DEAPIX200, DEAPIX500: we consider respectively a single black pixel, 50, 200 and 500 black pixels randomly scattered on the image DEAPIX-vcl: one black vertical line is drawn at the center of the image DEAPIX-3l: 2 horizontal black lines and 1 vertical black line are drawn
Flare	We use flare effects from the Automold [86] library	FLARE: we add flare with random position and angle
No Bayer filter	We convert the image to a numPy array and then we multiply it by [0.2989, 0.5870, 0.1140], which are weights for RGB-to-greyscale conversion [79]	NBAYF: We multiply all RGB pixels of the selected images by the scaling factor [0.2989, 0.5870, 0.1140]
No chromatic aberration correction	Image processing with PIL Image Module [12], numPy [13] and [68].	CHROMAB1-b, CHROMAB1-nb, CHROMAB2-b, CHROMAB2-nb: we introduce the effect of Chromatic Aberration for two incremental levels of aberration, with and without blur
No demosaicing	We create an image twice the size of the original one, and we map the RGB values from the original image according to the BGGR pattern in Fig. 2	DEMOS: the image is create twice the $(h, w)$ dimensions of the original image, with colours decomposed in a BGGR pattern
No noise reduction	Speckle noise is introduced using <code>cv2</code> [11] and numPy's <code>np.random.normal(0, i, img.size)</code> [13], with $i$ representing the noise level	NOISE: we add gaussian noise on the entire image, applying 10 different values for the Standard deviation (spread or "width") of the distribution, with $i$ ranging from 0.2 (very low noise) to 5 (excessive disturbance)
No sharpness correction	Sharpness is removed using the PIL <code>ImageEnhance</code> module ( <code>ImageEnhance.Sharpness</code> ) [12]	SHARP: the method is invoked with 6 different sharpness factors, ranging from -5 (severe loss of sharpness) until 0 (visual effect is similar to a light blur)

The object detectors are re-trained except DSGN and Disp R-CNN for computational load issues. In these last two cases we use instead the trained models provided by the authors. For each re-trained object detector, we verify that scores on the validation set are similar to those declared by their authors.

Each of the 130 failure configurations of Table II is applied on the 500 images of the validation set; all the resulting images (65000 i.e., 500×130) are available at [10].

All computations are performed on a Dell Precision 5820 Tower with a 12-Core I9-9920X and GPU Nvidia Quadro RTX5000.

**Results on clean images.** Results on clean images are in Table IV. Stereo object detectors DSGN and Disp R-CNN compute both bi-dimensional (2D) and tri-dimensional (3D) bounding boxes, measuring respectively 2D AP and 3D AP. Interestingly, Table IV shows that AP on clean images is not the highest AP, with the exception of SqueezeDet. We further investigate this, to verify if object detectors benefit of certain failure configurations.

We can disregard this hypothesis, because in general the improvements are just small fluctuations on the AP score, with the exception of DEAPIX-vcl on Disp R-CNN, which raises 3D AP of approximately 5 points (from ~58% to ~63%). We did further analysis on this failure configuration on other sets of KITTI images, and we measured 3D AP very similar to the 3D AP on clean images. Considering that we did not re-trained Disp R-CNN, the cause may simply be flukes in the selection of the validation set.

**Results on lens failures.** We discuss the simulated failures that affect lenses only i.e., brightness, blurred, broken lens, dirty, flare, rain.

Fig. 7 shows the AP recorded from the object detectors, under 10 different brightness failures. As expected, significant alterations of brightness drastically reduce the detection capability. Stereo object detectors better tolerate brightness alterations. This is because they use two cameras, leading to two parallel image sets, while our failure is injected only on one camera i.e., one of the two images set.

We obtain a similar effect with the 25 configurations of blurred failure (not shown for brevity). All algorithms reduce their detection capability as the amount of blur increases. Noteworthy, with BLUR configurations from (1, 1) to (5, 5), DSGN 2D and Disp R-CNN 2D present a minimal reduction of AP. Together with Fig. 7, this suggests that it is possible to tolerate light levels of blur and brightness alteration.

TABLE IV  
RESULTS ON CLEAN IMAGES AND MAXIMUM AP.

Algorithm	Metric	AP on clean images (%)	Max AP (%)	Failure configuration for Max AP
FastBox	2D AP	86,67	87,00	DIRTY
SqueezeDet	2D AP	87,50	87,50	---
SqueezeDet+	2D AP	88,61	88,87	BRIGHT 0,6
ResNet50	2D AP	88,30	88,94	SHARP 0
DSGN	2D AP	89,67	91,81	BLUR (2,2)
	3D AP	70,80	71,18	BRLE
Disp R-CNN	2D AP	89,94	90,08	SHARP 0
	3D AP	57,89	63,14	DEAPIX-vcl

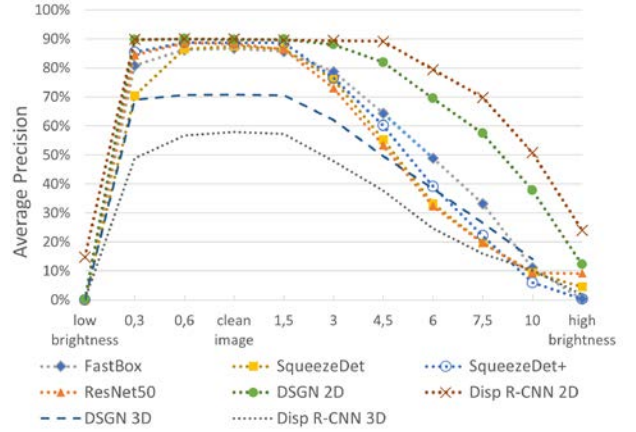


Fig. 7. AP measured for 10 different brightness alterations.

We comment instead on broken lens, dirty, and rain failures with the help of Table V. If the AP deviates of less than 5% from the AP on clean images, the corresponding cell in Table V is colored. These failures are simulated by overlaying images: clearly, the characteristics of the image that is overlaid has a relevant role on the measured AP e.g., because of the amount and size of raindrops contained. However, considering the average, we can deduce that most of the BRLE (scratches) and DIRTY failures are well-tolerated by most of the object detectors.

Last, flare effects we simulated lead to a significant AP reduction (from 8% in DSGN 2D, which records AP= 0,82, to above 44% with Squeeze, which scores AP= 0,60). Again, failure impact is reduced for stereo object detectors, because we inject in one of the two images set.

**Results on lens-camera body failures.** We discuss condensation and ice failures. Also in these cases, the AP reduction depends strongly on the overlaid figure e.g., the amount of ice crystals in the figure that is overlaid. In Fig. 8 we show the minimum AP recorded under ice and

TABLE V  
AP (IN PERCENTAGE) FOR BROKEN LENS, DIRTY AND RAIN.

	AP	BRLE %			DIRTY %			RAIN %		
		min	max	avg	min	Max	avg	min	max	avg
FastBox	2D	68	87	83	78	87	85	37	87	70
SqueezeDet	2D	71	87	84	82	87	86	26	87	67
SqueezeDet+	2D	75	89	87	78	89	88	37	89	74
ResNet50	2D	61	88	83	86	89	88	22	87	68
DSGN	2D	87	90	89	88	90	90	81	90	87
	3D	64	71	69	66	71	69	50	70	62
Disp R-CNN	2D	81	90	89	89	90	90	71	90	84
	3D	48	58	56	53	63	57	27	58	48

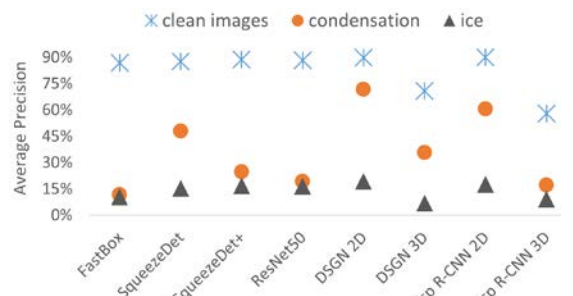


Fig. 8. Minimum AP with ice and condensation failures.

condensation failures. While all object detectors are severely affected by the ice failure, condensation effects vary significant from an object detector to the others. Again, as it can be expected, stereo object detectors tolerate failures affecting only one of the two cameras in case of 2D recognition.

**Results on bayer filter failures.** We consider the No Bayer Filter failure. This showed a peculiar behavior: the removal of colors according to a correction factor has a relevant impact on the various detectors, leading to a massive reduction of AP, which is measured below 10%. Additionally, execution of Disp R-CNN failed under such configuration. The exception is DSGN which just reduces 2D AP of 3% and 3D AP of 19%.

**Results on ISP failures.** Failures of the ISP that we simulate are banding, dead pixels, no chromatic aberration, no demosaicing, no noise reduction, no sharpness correction. The two configurations of the banding failure BAND1 and BAND2 are well-tolerated by the object detectors, leading to minimal AP reduction. The worst case is with ResNet50, where the AP is reduced from 88% with clean images to 84% in case of BAND2.

Also, dead pixel failures have limited effects on the image processing phase. In fact, for all the configurations DEAPIX1, DEAPIX50, DEAPIX200, DEAPIX500, DEAPIX-vcl, DEAPIX-3l, the worst AP reduction is with ResNet50, that is also in this case from 88% on clean images to 84% with the DEAPIX500 failure.

Instead, the failure no chromatic aberration correction is a serious concern as it generally leads to a severe loss in AP, also for stereo cameras. Table VI marks in dark gray the cases in which AP is reduced by above 50%, and in light grey the AP reduction between 20% to 50%.

The no demosaicing failure is rather tricky to simulate, and this is the reason some object detectors are not able to work properly with the demosaiced images. As discussed in Table II, to separate the RGB components, an image of larger scale is created, but object detectors are trained on images of different size. It is noteworthy that Disp R-CNN rates 89,46% 2D AP and 43,30% 3D AP, showing limited AP reduction with respect to the clean images. The other object detectors score 0% AP, except for DSGN which fails during execution: this happens due to the processing of pairs of images of different size.

Last, the two failures no noise reduction and no sharpness correction show predictable trends: incremental values of NOISE and SHARP slowly degrade performances.

TABLE VI  
AP (IN PERCENTAGE) FOR NO CHROMATIC ABERRATION.

	AP	CHROM	CHROM	CHROM	CHROM
		AB1-nb	AB1-b	AB2-nb	AB2-b
FastBox	2D	22,57%	9,62%	6,98%	0,74%
SqueezeDet	2D	28,76%	11,98%	7,59%	5,38%
SqueezeDet+	2D	42,15%	26,72%	15,97%	14,74%
ResNet50	2D	42,94%	13,22%	24,87%	9,67%
DSGN	2D	58,43%	58,97%	23,56%	29,44%
	3D	1,17%	1,00%	0,33%	0,68%
Disp R-CNN	2D	79,76%	60,51%	67,89%	37,63%
	3D	2,45%	3,03%	9,09%	9,09%

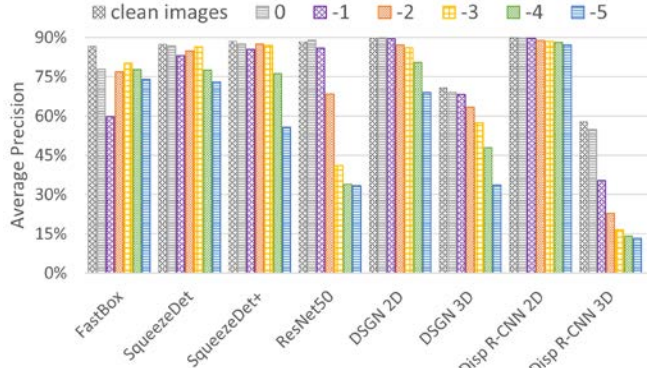


Fig. 9. Failure “no sharpness correction”: SHARP configurations

However, while NOISE leads progressively towards 0% AP, the AP reduction in case of severe unsharpened image is still mild especially under Disp R-CNN 2D. This is well-visible in Fig. 9.

**Summarizing comparison.** We investigate if an object detector is particularly more robust to camera failures than the others. For each object detector and each of the 130 failure configurations, we compute the difference between the AP on clean images and the AP for such failure configuration. Then we compare results for the different object detectors: If an object detector consistently records the lowest AP reduction, it means it is particularly more robust to camera failures.

Amongst object detectors for mono camera, FastBox has the lowest AP reduction in 50 cases out of 130, followed by SqueezeDet+ with 40 cases. Squeeze instead is the most robust in 25 cases, the majority of which are BLUR configurations. Amongst stereo approaches, the situation is well-balanced between DSGN and Disp R-CNN, which results the most robust respectively under 62 and 65 configurations (and 4 ex-aequo). In general, Disp R-CNN resulted more robust under BLUR and BRIGHT configurations, while DSGN on DIRT configurations. As evident, none of the object detectors is significantly more robust than the others.

## 5 EFFECTS ON DRIVING TASKS

To further understand the effects and the safety risk of the identified failures, we inject them in the vehicle camera of an autonomous driving simulator. Logs and some videos that describe the various runs are available at [10].

### 5.1 Autonomous Driving with Carla simulator

We opt for the Open Urban Driving Simulator Carla (Car Learning to Act, [1]) to create a vehicle that is autonomously driving in a town using only the RGB camera.

Carla has been implemented as an open-source layer over the Unreal Engine 4 (UE4, [2]) to support training, prototyping, and validation of autonomous driving models, including both perception and control. Carla includes urban layouts, several vehicle models, buildings, pedestrians, street signs, etc. Further, it provides information on the simulated vehicles as position, orientation, speed, acceleration, collisions and traffic violations.

Amongst the autonomous driving agents that exist for Carla, we use the trained agent from [3]. Technical details

on the trained agent are outside the scope of this paper and are reported in [3]; we introduce only the notions required to illustrate our tests. Using this trained agent, at each simulation step it is acquired: i) one RGB image from the frontal camera of the vehicle at a resolution of  $384 \times 160$  pixels (this is significantly smaller than the KITTI images used in Section 4), and ii) the current speed from the speed sensor. These values are processed by the trained agent to predict waypoints in the camera coordinates, and then these waypoints are projected into the vehicle's coordinate image [3]. In simpler words, the trained agent "designs" a trajectory composed of five waypoints on the image acquired from the camera. From this, a low-level controller is executed that decides the steering angle, the throttle level, and the braking force. Finally, throttle, speed and braking are applied on the vehicle.

We selected this trained agent amongst the various available because: i) it uses only the camera as sensing system; ii) it presents very good performances, with a minimal number of collisions. Further, the model was trained with image augmentations following [8], including pixel dropout, blurring, Gaussian noise, and color perturbations which partially overlap with our failures set.

## 5.2 Injection strategy and failure implementation

Our injection strategy consists of the following actions, performed at each simulation step: i) acquire the output image from the camera; ii) modify the image by injecting the selected failure before the trained agent processes the image; and iii) feed the modified image to the trained agent. For brevity, we report a subset of the failure configurations in Table III (simulations of a larger set are reported in our previous work [78]). We report on the injection of the following subset of failures configurations: BAND1, BRIGHT 0 (black images), BRIGHT 1.5, BLUR (12, 12), DEAPIX1, DEAPIX200, DEAPIX-vcl, NBAYF, CHROMAB2-nb, NODEMOS, NOISE 1, SHARP -3.5, one BRLE, one COND, one DIRTY, one ICE, one RAIN. The images overlaid for these tests are available at [9]. We exclude Flare as it depends on the sun position and it needs to consider vehicle movements, requiring environmental data; further, it would overlap with the flare effects already represented in the Carla simulator.

## 5.3 Test plan and execution

The test plan is based on the *corl2017* benchmark from [1]. The test plan is composed of multiple runs in which a target vehicle must reach a destination position  $B$  from a starting position  $A$  before a timeout expires. The timeout value is the time required to cover the distance from  $A$  to  $B$  at an average speed of 10 Km/h as in [1], [3]; this matches the settings of the *corl2017* benchmark, which takes into account vehicle stops at traffic lights and traffic. Re-using the nomenclature from [1], the starting position  $A$  and the destination position  $B$  are selected such that three *test objectives* are set:

- *Straight road*: Destination position  $B$  is located straight ahead of the starting position  $A$ .
- *Turn road*: Destination position  $B$  is one turn away from the starting position  $A$ .

- *Navigation*: There is no restriction on the location of the destination position  $B$  relative to the starting position  $A$ ; this results in runs of longer distance and multiple turns.

For each individual run, the success criterion is to reach the destination  $B$  before expiration of the timeout. The failure criterion is whenever the vehicle collides or the timeout expires: we modified the *corl2017* benchmark to halt the run whenever a collision occurs, as in our work we prioritize safety over travelled distance.

The target town we select is the Carla Town02, that is a basic town layout with all "T junctions" and it is also the town used for testing the trained agent in [3]. Further, we select three different weather conditions, that represent a clear noon, a wet cloudy noon, and a hard rain sunset. In addition, in each of the runs performed, the town includes exactly 50 vehicles and 30 pedestrians. We always use the same randomization seed so that spawning positions of vehicles and pedestrians are the same in the repeated runs.

The experiments were organized in two phases. In the first phase, we performed golden runs on clean images, i.e., we execute the simulation runs without introducing any modification to the images captured by the camera. The second phase repeats the same runs of the previous phase, but with the injection of camera failures to each acquired image.

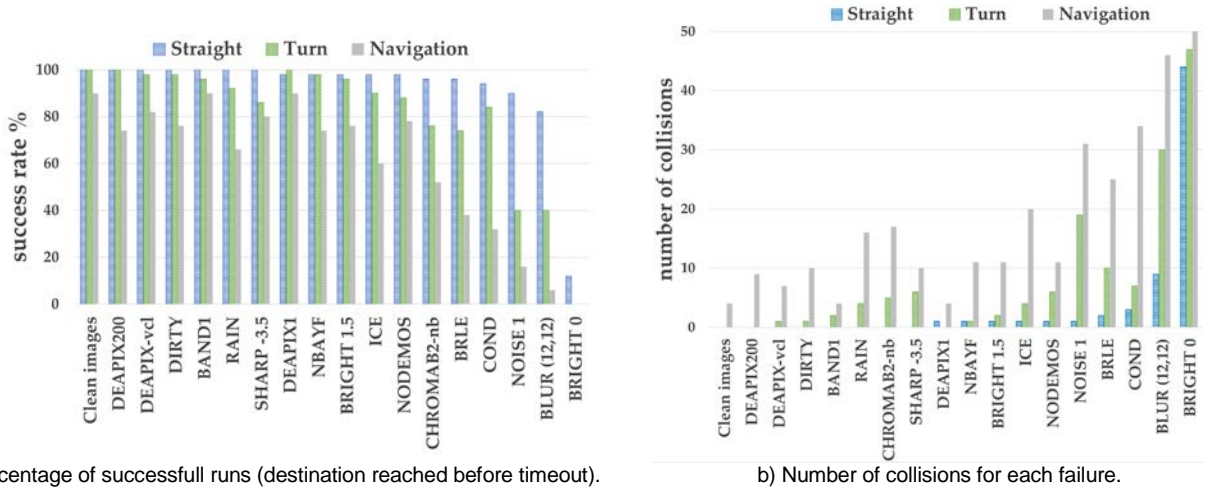
The three test objectives are investigated in 150 runs (50 runs for each test objective) for the golden runs and for the 17 failure configurations that we inject. With a total of 2700 runs, the simulated time in Carla corresponds to approximately 80 hours of driving. The simulations were executed on a Dell Precision 5820 Tower with a 24-Core I9-9920X and GPU Nvidia Quadro RTX5000.

## 5.4 Collisions and success rate

First, we discuss the impact of each individual failure on the decisions of the trained agent of [3]. Fig. 10a and Fig. 10b show respectively the success rate and the number of collisions for the three test objectives Straight road, Turn road and Navigation. Not surprisingly, runs on clean images perform the best, with the highest success rate and the lowest number of collisions (4 collisions, all under the Navigation test objective). Similar results are achieved by DEAPIX1 (5 collisions) and BAND (6 collisions): differences from the golden runs are small.

In fact, it is credible that DEAPIX1 does not affect significantly the trained agent: this failure consists in a single black pixel introduced at the bottom right of the image and, on top of this, the agent was trained with pixel dropout augmentation. Instead, it is a positive surprise that the trained agent is robust to banding i.e., horizontal and vertical lines overlaid to the image.

On the opposite, the failures BRIGHT 0, BLUR, NOISE1, COND, BRLE1 are the worst performing. In fact, these failures significantly modify the image. Still, they show some successful runs, and this may look especially surprising for the Straight road with White and Black failures. This is



a) Percentage of successful runs (destination reached before timeout).

b) Number of collisions for each failure.

Fig. 10. Execution of the simulated runs in the three test objectives Straight road, Turn road, and Navigation road.

simply because the car is moving forward blindly in a straight direction and, if there are no obstacles, the run ends successfully.

The remaining failures have variable performances, however for each of them the number of collisions is always the highest in Navigation and the lowest in Straight road, with irrelevant exceptions as DEAPIX-1 where there are 0 collisions in Turn road and 1 in Straight road. This trend fully matches the results of the golden runs.

Last, we observe that the order of failures in Fig. 10a and Fig. 10b is not the same. This is mostly because some runs terminate due to timeout: in general, a timeout occurs when the vehicle is unable to decide how to advance after a particular event e.g., after hard braking to avoid a vehicle in a colliding trajectory. Since this is not leading to collisions, we consider that timeouts occur in case of safe failures and we do not discuss them further.

**Impact on safety and generalization of results.** It is evident that our results depend on the target application, and consequently a univocal definition of failure criticalities and risks cannot be devised. However, these experiments bring evidence that the represented failures should not be ignored when building image-based autonomous driving systems and applications. In fact, we show that even failures with small visual effects affect the decisions of the trained agent, e.g., see the number of collisions under the DEAPIX200 failure that scatters 200 dead pixels on a camera with a resolution of  $384 \times 160$  (above 60.000 pixels).

## 8. RELATED WORKS

To the best of our knowledge, no research works discuss a complete failures model of a vehicle camera, including an analysis of effects and safety risks, and the provision of a software library. However, several works deal with similar or inherent problems.

The *performance, robustness, and security of an RGB camera* have been widely explored, however usually focusing on specific elements or target metrics and without addressing the full set of failures. For example, Bijelic et al. [25] present a test and evaluation methodology to compare sensor technologies: the paper shows the difference between an image

captured by a standard CMOS camera and one captured by a gated camera. Schops et al. [26], motivated by the limitations of existing multi-view stereo camera benchmarks (a stereo camera has two or more lenses, each with a separate image sensor: this allows the device to simulate binocular human vision and capture three-dimensional images [34]), introduce a new dataset and a technique to minimize the photometric errors. In [32] a simulation environment is presented which includes the virtual structures of a car designed for autonomous driving tests; typical driving situations have been used to analyze how sensors respond when used in real circumstances as well as to confirm the impacts of environmental conditions. Considering instead sensor security issues, Petit et al. [19] blind a commercial camera system used in commercial vehicles with several light sources. The work shows that leveraging a laser or LED matrix could blind the camera. Similarly, Yan et al. [34] successfully blind the camera by aiming the LED and the laser light at the camera directly: radiating a laser beam against a camera of a vehicle may cause irreversible damage and disrupt the corresponding autonomous applications. In general, it is observed that, because of the vulnerability of the camera caused by its optical characteristics, it is difficult to build a completely secure camera system [18].

In the domain of image-based AI/ML algorithms and applications, many works acknowledge that *the risk of accidental alterations of the output image of the camera is realistic* e.g., [47]. However, this consideration is usually ancillary to the main contribution of the work. Nonetheless, works in the AI/ML domain strongly helped us refining and cross-checking the completeness of the failure modes we identified. In fact, chromatic aberration, noise, color temperature, blur and brightness alteration are often considered in image-based AI/ML trained agents, although for the scope of data augmentation during training [30]. For example, Toromanoff et al. [31] present a new convolutional neural networks (CNN) model, in which label augmentation based on translation and rotation allows generating data using only a short-range fisheye (wide angle) camera. Menze et al. [23] elaborate a new model and data set for 3D scene flow estimation, and explicitly take

advantage of the background movement caused by the camera mounted on a vehicle. Behzadan et al. [24] show a new deep reinforcement learning framework; in order to develop robust sensors and algorithms, testing under certain meteorological conditions is deemed crucial for determining the impact of bad weather on sensors.

Several other works instead focused on *security and robustness of the trained agents that contribute to the autonomous driving system*, trying to understand the possible modification of camera images that could be produced by an attacker, or to define corner cases. Attackers may maliciously alter the images with transformations that are similar, in concept, to those that could happen with non-malicious failures: also, these works were useful when identifying the set of failures. Most relevant, K. Pei et al. [35] apply input space reduction techniques to transform the image, and can simulate a wide range of real-world distortions, noises, and deformations. W. Wu et al. [36] present a faults model for deep neural networks classifiers, which includes several corner cases based on the alteration of the input image, including amongst the possible causes brightness, camera alignment, and object movements. Finally, evasion attacks consist in modifying the input to a classifier such that it is misclassified, while keeping the modification as small as possible [37]. For example, to create such adversarial images, the correct images can be modified by overlaying carefully crafted noise [38], or altering few selected pixel [39], or with rotation and translation [40]. A representative list of such evasion attacks and their implementations is available at [37].

## 9. CONCLUSIONS

It is commonly acknowledged that RGB cameras may fail, and that a failed camera may produce altered images. This is a relevant issue if such images are further processed by safety-critical image-based applications. Nevertheless, to our knowledge, a thorough enumeration of camera failure modes and means for their reproduction are still missing. Especially when cameras are used for safety-critical applications e.g., in the autonomous driving domain, the definition of failure modes would benefit software and system engineers to build resilient architecture or to assess application robustness.

This paper discussed the failure modes of a vehicle camera, identified through the application of an FMEA and literature review. The discussion is complemented with the identification of potential mitigations, and with a public library that can be used to reproduce the failures on images sets. Further, we reproduced such failures in image-based AI/ML applications for autonomous driving (six car detectors and one self-driving agent), to understand failures impact. Although results are obviously application-dependent, it is clear that even failures that slightly perturb the image may alter the decisions of a trained agent.

## ACKNOWLEDGMENT

This work has been partially supported by the H2020 programme under the Marie Skłodowska-Curie grant

agreement 823788 (ADVANCE) project.

## REFERENCES

- [1] Dosovitskiy, Alexey and Ros, German and Codevilla, Felipe and Lopez, Antonio and Koltun, Vladlen, "CARLA: An Open Urban Driving Simulator", Conference on Robot Learning, pp1–16, 2017.
- [2] Unreal Engine, [www.unrealengine.com](http://www.unrealengine.com) [last accessed 20 May 2020]
- [3] Chen Dian et al., "Learning by Cheating", Conference on Robot Learning (CoRL), 2019.
- [4] Huang, Jia, et al. "Failure mode and effect analysis improvement: A systematic literature review and future research agenda." Reliability Engineering & System Safety (2020): 106885.
- [5] Bouti, Abdelkader, and Daoud Ait Kadi. "A state-of-the-art review of FMEA/FMECA." International Journal of reliability, quality and safety engineering 1.04 (1994): 515-543.
- [6] Allen, Elizabeth, and Sophie Triantaphillidou. The manual of photography. CRC Press, 2012.
- [7] Guy, N. K. The Lens: A Practical Guide for the Creative Photographer. Rocky Nook, Inc., 2012
- [8] Codevilla, Felipe, et al. "End-to-end driving via conditional imitation learning." IEEE International Conference on Robotics and Automation (ICRA). IEEE, 2018.
- [9] [https://github.com/francescosecchi/Python\\_Image\\_Failures](https://github.com/francescosecchi/Python_Image_Failures)
- [10] <https://drive.google.com/drive/folders/1M5itBeFA6p7-pY-jSuVZ3IFBi6fMNIfek?usp=sharing>
- [11] CV2 filtering, <https://docs.opencv.org/2.4/modules/imgproc/doc/filtering.html> (last accessed 21 May 2020)
- [12] PIL 3.0, <https://pillow.readthedocs.io/en/3.0.x/> (last accessed 21 May 2020)
- [13] NumPy, <https://numpy.org/> (last accessed 21 May 2020)
- [14] Teng, Sheng-Hsien Gary, and Shin-Yann Michael Ho. "Failure mode and effects analysis." International journal of quality & reliability management (1996).
- [15] Premebida, Cristiano, Gledson Melotti, and Alireza Asvadi. "RGB-D Object Classification for Autonomous Driving Perception." RGB-D Image Analysis and Processing. Springer, Cham, 2019. 377-395.
- [16] Levinson, Jesse, et al. "Towards fully autonomous driving: Systems and algorithms." 2011 IEEE Intelligent Vehicles Symposium (IV). IEEE, 2011.
- [17] Lin, Shih-Chieh, et al. "The architectural implications of autonomous driving: Constraints and acceleration." Proceedings of the 23rd International Conference on Architectural Support for Programming Languages and Operating Systems. 2018.
- [18] Ren, Kui, et al. "The Security of Autonomous Driving: Threats, Defenses, and Future Directions." Proceedings of the IEEE (2019).
- [19] Petit, Jonathan, et al. "Remote attacks on automated vehicles sensors: Experiments on camera and lidar." Black Hat Europe 11 (2015): 2015.
- [20] Hagiwara, Hiroyuki. "Zoom lens and electronic apparatus." U.S. Patent No. 9,541,768. 10 Jan. 2017.
- [21] Hughes, C., et al. "Wide-angle camera technology for automotive applications: a review." IET Intelligent Transport Systems 3.1 (2009): 19-31.
- [22] Chung, Soon-Wook, Byoung-Kwang Kim, and Woo-Jin Song. "Removing chromatic aberration by digital image processing." Optical Engineering 49.6 (2010): 067002.
- [23] Menze, Moritz, and Andreas Geiger. "Object scene flow for autonomous vehicles." Proceedings of the IEEE conference on computer vision and pattern recognition. 2015.

- [24] Behzadan, Vahid, and Arslan Munir. "Adversarial reinforcement learning framework for benchmarking collision avoidance mechanisms in autonomous vehicles." *IEEE Intelligent Transportation Systems Magazine* (2019).
- [25] Bijelic, Mario, Tobias Gruber, and Werner Ritter. "Benchmarking image sensors under adverse weather conditions for autonomous driving." 2018 IEEE Intelligent Vehicles Symposium (IV). IEEE, 2018.
- [26] Schops, Thomas, et al. "A multi-view stereo benchmark with high-resolution images and multi-camera videos." *Proceedings of the IEEE Conference on Computer Vision and Pattern Recognition*. 2017.
- [27] Phillips, Jonathan B., and Henrik Eliasson. *Camera image quality benchmarking*. John Wiley & Sons, 2018.
- [28] AXIS Q60 PTZ, <https://www.axis.com/it-it/products/axis-q60-series> [last accessed 25 May 2020]
- [29] Guo, Longxiang, et al. "Automatic sensor correction of autonomous vehicles by human-vehicle teaching-and-learning." *IEEE Transactions on Vehicular Technology* 67.9 (2018): 8085-8099.
- [30] Carlson, Alexandra, et al. "Modeling Camera Effects to Improve Visual Learning from Synthetic Data." *Proceedings of the European Conference on Computer Vision (ECCV)*. 2018.
- [31] Toromanoff, Marin, et al. "End to end vehicle lateral control using a single fisheye camera." *IEEE/RSJ International Conference on Intelligent Robots and Systems (IROS)*. IEEE, 2018.
- [32] Hossain, Sabir, et al. "CAIAS simulator: self-driving vehicle simulator for AI research." *International Conference on Intelligent Computing & Optimization*. Springer, Cham, 2018.
- [33] Zheng, Zejia, Xie He, and Juyang Weng. "Approaching camera-based real-world navigation using object recognition." *Procedia Computer Science* 53 (2015): 428-436.
- [34] Yan, Chen, Wenyuan Xu, and Jianhao Liu. "Can you trust autonomous vehicles: Contactless attacks against sensors of self-driving vehicle." *DEF CON 24.8* (2016): 109.
- [35] Pei, Kexin, et al. "Towards practical verification of machine learning: The case of computer vision systems." *arXiv preprint arXiv:1712.01785* (2017).
- [36] Wu, Weibin, et al. "Deep validation: Toward detecting real-world corner cases for deep neural networks." *49th Annual IEEE/IFIP International Conference on Dependable Systems and Networks (DSN)*. IEEE, 2019.
- [37] Nicolae, Maria-Irina, et al. "Adversarial Robustness Toolbox v0.4.0." *arXiv preprint arXiv:1807.01069* (2018).
- [38] Moosavi-Dezfooli, Seyed-Mohsen, Alhussein Fawzi, and Pascal Frossard. "Deepfool: a simple and accurate method to fool deep neural networks." *Proceedings of the IEEE conference on computer vision and pattern recognition*. 2016.
- [39] Vargas, D. V., and Kotyan, S. "Robustness Assessment for Adversarial Machine Learning: Problems, Solutions and a Survey of Current Neural Networks and Defenses." *arXiv preprint arXiv:1906.06026* (2019).
- [40] Engstrom, Logan, et al. "A rotation and a translation suffice: Fooling cnns with simple transformations." *arXiv preprint arXiv:1712.02779* 1.2 (2017): 3.
- [41] Northrup, T. Tony Northrup's photography buying guide: How to choose a camera, lens, tripod, flash, & more, Waterford, Mason Press, 2016.
- [42] Poli, P. *Fotografia digitale: guida completa*, Apogeo, Milano, 2014.
- [43] Townsend, Herbert E. "Outdoor atmospheric corrosion." *ASTM*, 2002.
- [44] Elkins, David E. *The camera assistant's manual*. Taylor & Francis, 2013.
- [45] Cai, Jian-Feng, et al. "Blind motion deblurring from a single image using sparse approximation." 2009 IEEE Conference on Computer Vision and Pattern Recognition. IEEE, 2009.
- [46] Fang, Lu, et al. "Separable kernel for image deblurring." *Proceedings of the IEEE Conference on Computer Vision and Pattern Recognition*. 2014.
- [47] Gu, Jinwei, et al. "Removing image artifacts due to dirty camera lenses and thin occluders." *ACM Transactions on Graphics (TOG)* 28.5 (2009): 1-10.
- [48] Eigen, David, Dilip Krishnan, and Rob Fergus. "Restoring an image taken through a window covered with dirt or rain." *Proceedings of the IEEE international conference on computer vision*. 2013.
- [49] Chabert, Floris. *Automated lens flare removal*. Technical report, Stanford University, Department of Electrical Engineering, 2015.
- [50] Kondou, Masayoshi. "Condensation prevention camera device." U.S. Patent No. 9,525,809. 20 Dec. 2016.
- [51] Loiacono, Dominick F. "Noncondensing security camera housing window assembly." U.S. Patent Application No. 12/433,457.
- [52] Englander, Benjamin. "Video camera unit, protective enclosure and power circuit for same, particularly for use in vehicles." U.S. Patent No. 5,455,625. 3 Oct. 1995.
- [53] Talbert, Abrams, Milford B. Moore, and Nelson Roy. "Lens heater." U.S. Patent No. 2,442,913. 8 Jun. 1948.
- [54] Riffe, William J., and Jack D. Carter. "Method for the prevention of fouling and/or corrosion of structures in seawater, brackish water and/or fresh water." U.S. Patent No. 5,346,598. 13 Sep. 1994.
- [55] Zamfir, Adrian, et al. "An optical model of the appearance of blemishes in digital photographs." *Digital Photography III*. Vol. 6502. International Society for Optics and Photonics, 2007.
- [56] Steinberg, Eran, Petronel Bigioi, and Adrian Zamfir. "Detection and removal of blemishes in digital images utilizing original images of defocused scenes." U.S. Patent No. 7,295,233. 13 Nov. 2007.
- [57] Cho, Chao-Yi, et al. "Real-time photo sensor dead pixel detection for embedded devices." 2011 International Conference on Digital Image Computing: Techniques and Applications. IEEE, 2011.
- [58] Dong, Kimble. "On-chip dead pixel correction in a CMOS imaging sensor." U.S. Patent No. 7,522,200. 21 Apr. 2009.
- [59] Wikipedia, "Dithering." <https://it.wikipedia.org/wiki/Dithering> [last accessed May 2020].
- [60] Barrett, S. *Environmental Engineering Considerations and Laboratory Tests*. MIL-STD-810G, 2008.
- [61] B. Grossmann and Y. C. Eldar. "An efficient method for demosaicing" in 2004 23rd IEEE Convention of Electrical and Electronics Engineers in Israel, pp. 436-439, Sep 2004.
- [62] Lilon, S. H. I., and Ilia Ovsianikov. "Demosaicing rgbz sensor." U.S. Patent Application No. 13/944,859.
- [63] Baek, Yeul-Min, et al. "Noise reduction for image signal processor in digital cameras." 2008 International Conference on Convergence and Hybrid Information Technology. IEEE, 2008.
- [64] Yoneyama, Satoru, et al. "Lens distortion correction for digital image correlation by measuring rigid body displacement." *Optical engineering* 45.2 (2006): 023602.
- [65] Prescott, B., and G. F. McLean. "Line-based correction of radial lens distortion." *Graphical Models and Image Processing* 59.1 (1997): 39-47.
- [66] Sawhney, Harpreet S., and Rakesh Kumar. "True multi-image alignment and its application to mosaicing and lens distortion correction." *IEEE Transactions on Pattern Analysis and Machine Intelligence* 21.3 (1999): 235-243.

- [67] Kang, Sing Bing. "Automatic removal of chromatic aberration from a single image." 2007 IEEE Conference on Computer Vision and Pattern Recognition. IEEE, 2007.
- [68] Realistic Lens Blur/Chromatic Aberration Filter, <https://github.com/yoonsikp/kromo> [last accessed 23 May 2020]
- [69] Kim, Tai-hoon, et al., eds. Computer Applications for Web, Human Computer Interaction, Signal and Image Processing, and Pattern Recognition: International Conferences, SIP, WSE, and ICHCI 2012, Held in Conjunction with GST 2012, Jeju Island, Korea, November 28-December 2, 2012. Proceedings. Vol. 342. Springer, 2012.
- [70] Floyd F. Sabins, Jr., James M. Ellis, Remote Sensing: Principles, Interpretation, and Applications, Fourth Edition, Waveland Press, 2020.
- [71] Baumgartner, Daniel, et al. "Benchmarks of low-level vision algorithms for DSP, FPGA, and mobile PC processors." Embedded Computer Vision. Springer, London, 2009. 101-120.
- [72] Sharma, G. Photography Redefined, Lulu.com, 2013.
- [73] Bhargava, S. C., Electrical Measuring Instruments and Measurements, CRC Press, 2012.
- [74] Kelby, S. Scott Kelby's Digital Photography Boxed Set, Parts 1, 2, 3, 4, and 5, Peachpit Press, 2014.
- [75] Geiger, Andreas, Philip Lenz, and Raquel Urtasun. "Are we ready for autonomous driving? the kitti vision benchmark suite." 2012 IEEE Conference on Computer Vision and Pattern Recognition. IEEE, 2012.
- [76] Menze, Moritz, and Andreas Geiger. "Object scene flow for autonomous vehicles." Proceedings of the IEEE conference on computer vision and pattern recognition. 2015.
- [77] Everingham, Mark, et al. "The pascal visual object classes (voc) challenge." International journal of computer vision 88.2 (2010): 303-338.
- [78] Secci, Francesco, and Andrea Ceccarelli. "On failures of RGB cameras and their effects in autonomous driving applications." The 31st International Symposium on Software Reliability Engineering (ISSRE 2020), pp. 13-24, 2020. IEEE.
- [79] International Telecommunication Union (ITU). "BT.601: Studio encoding parameters of digital television for standard 4:3 and wide screen 16:9 aspect ratios", 2011.
- [80] eval\_kitti, [https://github.com/cguindel/eval\\_kitti](https://github.com/cguindel/eval_kitti)
- [81] Teichmann, Marvin, et al. "Multinet: Real-time joint semantic reasoning for autonomous driving." 2018 IEEE Intelligent Vehicles Symposium (IV). IEEE, 2018.
- [82] KittiBox, <https://github.com/MarvinTeichmann/KittiBox>
- [83] Wu, Bichen, et al. "Squeezedet: Unified, small, low power fully convolutional neural networks for real-time object detection for autonomous driving." Proceedings of the IEEE Conference on Computer Vision and Pattern Recognition Workshops. 2017.
- [84] Iandola, F. N., Han, S., Moskewicz, M. W., Ashraf, K., Dally, W. J., & Keutzer, K. (2016). SqueezeNet: AlexNet-level accuracy with 50x fewer parameters and < 0.5 MB model size. arXiv preprint arXiv:1602.07360.
- [85] He, Kaiming, et al. "Deep residual learning for image recognition." Proceedings of the IEEE conference on computer vision and pattern recognition. 2016.
- [86] Automold, <https://github.com/UjjwalSaxena/Automold--Road-Augmentation-Library>
- [87] Chen, Yilun, et al. "Dsgn: Deep stereo geometry network for 3d object detection." Proceedings of the IEEE/CVF Conference on Computer Vision and Pattern Recognition. 2020.
- [88] Sun, Jiaming, et al. "Disp R-CNN: Stereo 3D Object Detection via Shape Prior Guided Instance Disparity Estimation." Proceedings of the IEEE/CVF Conference on Computer Vision and Pattern Recognition. 2020.
- [89] He, Kaiming, et al. "Mask r-cnn." Proceedings of the IEEE international conference on computer vision. 2017.
- [90] Peiliang Li, Xiaozhi Chen, and Shaojie Shen. Stereo r-cnn based 3d object detection for autonomous driving. In Proceedings of the IEEE Conference on Computer Vision and Pattern Recognition, pages 7644-7652, 2019
- [91] ActionVFX, <https://www.actionvfx.com/>

**Andrea Ceccarelli** received the PhD in Informatics and Automation Engineering from the University of Florence, Florence, Italy, in 2012. He is currently a Research Associate of Computer Science at the same University. His primary research interests are in the design, monitoring and experimental evaluation of dependable and secure systems, and systems-of-systems. His scientific activities originated more than 100 papers which appeared in international conferences, workshops, and journals.

**Francesco Secci** graduated from the University of Florence, Florence, Italy, very recently, in 2020. Since graduating, he has been working and researching on safety-critical systems, mainly experiencing with the Factory 4.0 domain.